A Measurement of the Parity Violating Proton Asymmetry in the Capture of Polarized Cold Neutrons on ^3He.

A Proposal

Submitted to the SNS FNPB PRAC

November 15, 2007

J.D. Bowman (**PI**), Oak Ridge National Laboratory, Oak Ridge, TN 37831, USA
R. Carlini, Jefferson National Laboratory, Newport News, VA 12002, USA
C. Crawford (**PI**), University of Kentucky, Lexington, KY 40506 USA
M.T. Gericke (**PI**), University of Manitoba, Winnipeg, MB, Canada R3T 2N2
C. Gillis, Indiana University, Bloomington, IN 47408
C .Gould, NC State University, Raleigh, NC 27695
V. Gudkov, University of South Carolina, Columbia, SC 29208
J. Martin, University of Winnipeg, Winnipeg, MB, Canada R3B 2E9
A. Micherdzinska, University of Winnipeg, Winnipeg, MB, Canada R3B 2E9
S.A. Page, University of Manitoba, Winnipeg, MB, Canada R3T 2N2
S.I. Penttilä, Oak Ridge National Laboratory, Oak Ridge, TN 37831, USA
M. Viviani, INFN, Sezione di Pisa, Pisa, 56127, ITALY

Abstract

We propose a measurement the parity violating asymmetry A_p of the correlation between the longitudinal polarization of incoming cold neutrons ($\vec{\sigma}_n$) and the outgoing momentum of protons ($\vec{k}_p$) after nuclear breakup in the reaction $\vec{n} +^3 He \rightarrow p + T + 765$ keV. The asymmetry is directly related to the weak nucleon-nucleon coupling which is of fundamental interest in the verification of the meson exchange model of NN interactions, as well as in the verification of several emerging χ_{PT} based effective field theory models. The reaction is well suited to these purposes because the PV asymmetry is expected to be large and the nuclear structure can be accurately treated using few-body methods. Testing these models can provide new and important information about QCD at low energy and how it modifies the weak interaction. We estimate the size of the asymmetry to be around 3×10^{-7}, based on estimates, scaling from p-p scattering, in the scattering states, and a calculation of the bound state asymmetry. We argue that it is possible to measure the asymmetry to an accuracy of about 2×10^{-8} in $\approx 10^7$ sec. We provide a reference design of the experiment and show that it is possible to construct it, using the same technology which has been used for many other cold neutron experiments. The only exception to that is a ^3He ion chamber serving as a combined target and detector, which is based on well known technology. We present an overview of the theoretical background and motivation, including a short discussion of a new (in progress), detailed calculation of the asymmetry and its relation to the coupling constants. We also provide an analysis of the associated systematic effects.

1 Introduction

The importance of the study of the hadronic weak interaction between nucleons (the weak NN interaction) has been outlined in various recent publications [1, 2, 3]. At the heart of this effort lies the desire to understand the weak interaction between quarks, which has been hampered by the challenge to separate the weak effects from the much larger strong effects in the non-perturbative QCD (strong coupling) limit. The study of the hadronic weak interaction is of great relevance for low energy, non-perturbative QCD. The properties of quark-gluon wave functions of hadrons are not well understood theoretically and have only partially been tested experimentally at low energy. The hadronic weak couplings probe short range correlations between quarks because the quark-quark weak interaction occurs when the distance between quarks is $\leq 2 \times 10^{-3}$ fm.

Over the past 40 years, since the first observation of parity violation between nucleons in nuclei [4], there has been intense effort on both the experimental and the theoretical side, to gain a better understanding of the weak NN interaction. Calculations of strangeness changing and conserving hadronic weak interaction processes and observables have been carried out for a long time [5, 6, 7], resulting in the so called weak meson exchange model, in which, at one vertex, the quarks of a nucleon couple weakly via Z, or W boson exchange to the quarks of a meson which then couples strongly to the other nucleon, at the other vertex. In 1980, Desplanques, Donoghue and Holstein (DDH) [8] published a calculation in which they used the quark model and SU(6) symmetry arguments relating the NN weak matrix elements to measured hyperon decay amplitudes, thereby bypassing the need for detailed knowledge of nucleon wave functions, to predict values for the parity violating weak hadronic couplings. According to these calculations, the weak parity-violating nucleon-nucleon interaction could be described by a meson-exchange potential involving seven weak meson-nucleon coupling constants, as shown in table 1.

Weak Meson-Nucleon Coupling Constants								
Coupling	**Cabbibo**				**Weinberg-Salam**			
	Range			Best Value	Range			Best Value
h_π^1	0	$\rightarrow$	1	0.5	0	$\rightarrow$	30	12
h_ρ^0	-64	$\rightarrow$	16	-25	-81	$\rightarrow$	30	-30
h_ρ^1	-0.7	$\rightarrow$	0	-0.4	-1	$\rightarrow$	0	-0.5
h_ρ^2				-58	-20	$\rightarrow$	-29	-25
h_ω^0	-22	$\rightarrow$	6	-6	-27	$\rightarrow$	15	-5
h_ω^1	-2	$\rightarrow$	6	-1	-5	$\rightarrow$	-2	-3
$h_\omega^{1'}$	Not Reported				Not Reported			

Table 1: DDH "best" value and reasonable ranges for six of the seven weak meson-nucleon coupling constants. Values are given in units of $1/g_{\pi NN}$ ($g_{\pi NN} = 3.8 \times 10^{-8}$).

The so-called DDH "reasonable ranges" and "best values" for seven (π, ρ, ω) weak meson nucleon couplings has been a defacto benchmark for comparison with experiment. However, in recent years this calculation has come under increased scrutiny. As pointed out in [2], for example, "the effects of chiral symmetry breaking on the value of h_π^1, which are not not included in the DDH treatment, may be anomalously large" [9].

New efforts to calculate parity violating observables starting from effective field theory Lagrangian (some based on χPT) are being undertaken, but non of them are currently at a stage where accurate calculations could be made to relate them to modern NN potentials, in a four nucleon system [10]. In pion-less effective field theory (which is the relevant one for this process), five independent couplings (or amplitudes) are generated ($\lambda_t, \lambda_s^{I=0,1,2}, \rho_t$), corresponding to the PV mixing of partial waves ${}^3S_1(I=0) \leftrightarrow {}^1P_1(I=0)$, ${}^1S_0(I=0,1,2) \leftrightarrow {}^3P_0(I=0,1,2)$, and ${}^3S_1(I=0) \leftrightarrow {}^3P_1(I=1)$ respectively [1].

Since the spin and iso-spin $S(I)$ of the initial $(n, {}^3He)$ and final (p,T) states are $(\frac{1}{2}(\frac{1}{2}), \frac{1}{2}(\frac{1}{2}))$ and $(\frac{1}{2}(\frac{1}{2}), \frac{1}{2}(\frac{1}{2}))$ respectively, and since these couple to intermediate ${}^3He\ 0^+(0)$ states, the possible mixing appears to be restricted to the ${}^1S_0(I=0) \leftrightarrow {}^3P_0(I=0)$ partial waves, based upon which one might expect the dominant contribution to the proton asymmetry to come from the $\lambda_s^{I=0}$ coupling. One arrives at the same conclusion when only parity mixing between bound states within the ${}^4He$ nucleus is considered (see below). In the DDH framework, the asymmetry is sensitive to a linear combination of the $\Delta I = 0$ ρ and ω couplings.

Clearly, whether it is the DDH framework or new EFT calculations that are being used, the exploration of the hadronic weak interaction remains an important and unresolved task. Based on the DDH model, Adelberger and Haxton [11] outline several possible experiment, some of which are in progress while others are being proposed. Unfortunately, progress in understanding the hadronic weak interaction has been slow, in spite of strong experimental activity. A number of recent reviews [13, 14] come essentially to the same conclusion, that the weak NN couplings are unknown. The reasons for the slow advance are both theoretical and experimental. On the experimental side, the challenge is to find feasible few nucleon experiments which can measure the various observables with high enough accuracy and together over-constrain the theoretical couplings. Problems in reaching the needed experimental accuracy stem from the small size of the weak amplitudes, as compared to the strong amplitudes. The small size of the measured asymmetries requires tight control of systematic effects and maximum possible efficiency to reduce the often long run time.

We argue in this proposal that the measurement of the proton asymmetry from neutron capture on ${}^3He$ is a relatively simple, straight forward and effective experiment. With the exception of a combined target-detector ion chamber, the experiment will use standard instruments, using technology that is identical to that used successfully in other experiments already.

2 The Experimental Observable (Estimates and Calculations)

We propose a measurement the parity violating asymmetry A_p of the correlation between the longitudinal polarization of incoming cold neutrons ($\vec{\sigma}_n$) and the outgoing momentum of protons ($\vec{k}_p$) after nuclear breakup in the reaction $\vec{n} + ^3He \rightarrow p + T + 765$ keV. In lieu of a detailed calculation (but see below), we estimate the size of the asymmetry in two ways: 1) we obtain a value of the RMS size of the asymmetry from the bound states, by estimating the PV mixing matrix element from the measured spreading width of the hadronic weak interaction (HWI) [15], and using a general expression for the ratio of PV and PC strong matrix elements in terms of the proton momentum and the charge radius of the helium nucleus [16] and 2) we consider parity mixing in the scattering states and estimate this contribution by scaling the measured asymmetry in $p-p$ scattering. To obtain a more concrete result for the size of the asymmetry, a detailed calculation, involving effective NN interaction models, is needed. Such a calculation is currently underway [17] and will also establish the asymmetry in terms of the DDH coupling constants.

2.1 Asymmetry Size Estimates

In general, the cross-section for the process at hand, containing parity mixing to first order, can be expressed as

$$\frac{d\sigma}{d\Omega} \propto |\langle\psi_{f0}|H_s|\psi_{i0}\rangle|^2 \left[1 + \alpha_{PV} \frac{|\langle\psi_{f1}|H_s|\psi_{i0}\rangle + \langle\psi_{f0}|H_s|\psi_{i1}\rangle|}{|\langle\psi_{f0}|H_s|\psi_{i0}\rangle|}\right] \tag{1}$$

where $|\psi_i\rangle = |\psi_{i0}\rangle + \alpha_{PV}|\psi_{i1}\rangle$ and $|\psi_f\rangle = |\psi_{f0}\rangle + \alpha_{PV}|\psi_{f1}\rangle$ are the first order parity mixed four nucleon states in the initial and final states. From this, the usual expression for the asymmetry is extracted.

$$A_{PV} = \alpha_{PV} \frac{|\langle\psi_{f1}|H_s|\psi_{i0}\rangle + \langle\psi_{f0}|H_s|\psi_{i1}\rangle|}{|\langle\psi_{f0}|H_s|\psi_{i0}\rangle|} = \alpha_{PV} \frac{|\langle f||Q_{PV}||i\rangle|}{|\langle f||Q_{PC}||i\rangle|} \cos\theta_{\sigma_n,k_p} \tag{2}$$

The ratio of strong matrix elements is generally quite hard to calculate, but Bunakov and Gudkov [16] argue that this can be approximated with

$$\frac{|\langle f||Q_{PV}||i\rangle|}{|\langle f||Q_{PC}||i\rangle|} \approx k_p r \approx 0.3 \ . \tag{3}$$

The $^3He(n,p)T$ reaction is due to a $(0^+, I=0)$ resonance in the compound ^4He nucleus at 20.21 MeV above the ground state [18]. The weak interaction can mix the 20.21 MeV resonance with the closest $(0^-, I=0)$ resonance at 21.01 MeV. The size of the PV mixing amplitude $\alpha_{PV} = \langle f|W|i\rangle/\Delta E$ can be estimated from the hadronic weak spreading width [15]

$$\Gamma_W = \frac{2\pi M_{rms}^2}{D} = (1.8^{+0.4}_{-0.3}) \times 10^{-7} eV \ ,$$

where $M_{rms} \approx \langle f|W|i\rangle$, $D \approx 20$ MeV is the energy difference between (0^+) states and $\Delta E \approx$ 800 keV, the difference between the parity mixed states. So that the expected size of the asymmetry from mixing between bound states is approximately given by

$$\begin{aligned} A_{PV} &\approx \alpha_{PV} k_p r \cos\theta_{\sigma,k_p} \\ &\approx 3 \times 10^{-7} \cos\theta_{\sigma,k_p} \ . \end{aligned}$$

The asymmetry in the scattering states can be estimated by scaling the measured $p-p$ asymmetry ($A_{pp} = 1.5 \times 10^{-7}$) from $T_{cm} = 22.5$MeV to the momentum of the proton ($\simeq 570$ keV) in the reaction considered here.

$$A_{PV} = A_{pp} \frac{2\sqrt{.6 \text{ MeV}}}{\sqrt{22.5 \text{ MeV}}} = 5 \times 10^{-8} \tag{4}$$

Neither of the above estimates involve any consideration of the interference between different components of the resonance or of the scattering-state wave functions. Each estimate is of the

RMS value of the asymmetry. When the two estimates are added in quadrature, the resonance mixing dominates and gives an estimated RMS size of the asymmetry of $\simeq 3 \times 10^{-7}$. We argue below that we can measure the asymmetry with a combined statistical and systematic uncertainty of $\simeq 2 \times 10^{-8}$ in a 10^7 second run at the FNPB. Thus the proposed measurement has two attractive features. 1) The uncertainty in the asymmetry is small, $\simeq 7\%$ of the estimated asymmetry. 2) We are studying a mass-4 system where the strong interaction can be treated using modern few body techniques. The theoretical uncertainty may be small for either the EFT or DDH approach.

2.2 New Calculations

A new calculation is currently under way [17] to calculate the proton asymmetry. The calculation is similar to the one presented in [19]. Here, scattering wavefunctions are computed using parity conserving nucleon-nucleon interactions and parity violation will be treated in first order perturbation. The so called Kohn variational principle will be used to relate the parity violating S-matrix elements to the parity violating potential (i.e the DDH potential).

3 Experimental Overview

Figure 1 shows a simple block diagram of the experiment. The neutron beam will be polarized by a remnant super-mirror polarizer. The initial polarization is transverse. The neutron spin then rotates adiabatically to be longitudinal, as it enters the longitudinal holding field of the experiment. The spin of the neutron will then be reversed to point either along or against the direction of momentum, using a spin rotator. The longitudinally polarized neutrons will capture in a thick ^3He ion chamber which is mostly sensitive to the number of forward going protons. It turns out that the first few wire planes in the chamber will not contribute in a statistically significant way to the asymmetry measurement, since there the sensitivity to longitudinal protons is small (see section 4.3). These wire planes however, receive the largest rate of neutron capture and can be used to normalize the signal. The detector is therefore self normalizing and does not require separate measurement of the beam flux. The longitudinal beam polarization is necessary to suppress systematic effects from parity allowed asymmetries (see the systematics section below).

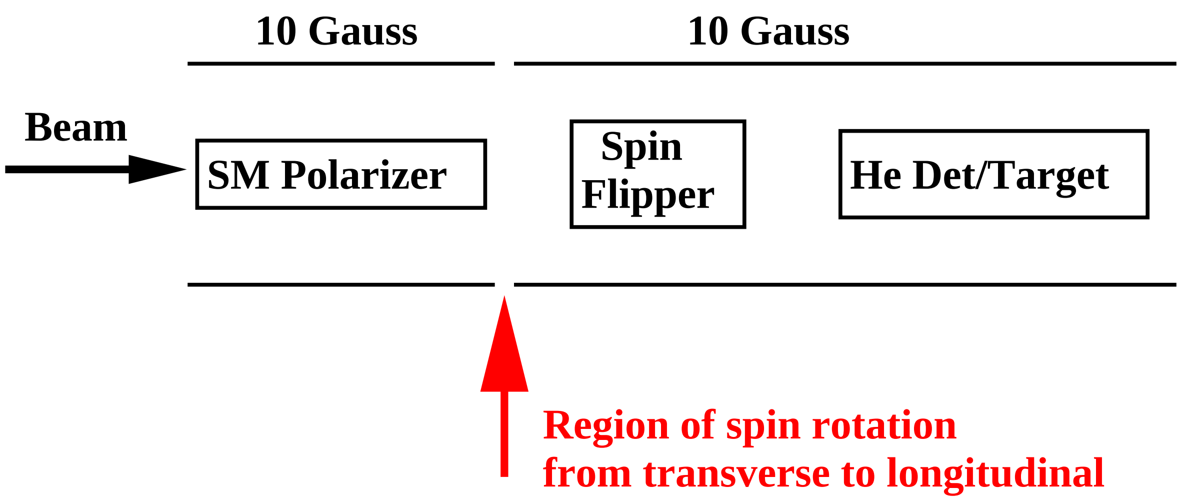

Figure 1: Schematic of the experimental layout.

4 Target / Detector Wire Chamber

4.1 Operating Principle and Design of ^3He Chambers

The operating principle of the target-detector wire chamber for this experiment is identical to that for a set of parallel plate ion chambers which were used for the NPDGamma experiment at Los Alamos, to measure the beam polarization and flux in-situ. (Similar, but more precise ones, better suited for high precision polarimetry and flux measurements, are currently being developed for the FNPB beam line.) Figure 2 [20] shows a schematic of the neutron beam monitors.

The beam monitors consist of three parallel plate electrodes enclosed in an aluminum housing and operate as follows: A neutron enters the monitor and encounters a gas consisting mostly of Nitrogen, with traces of helium 3 and helium 4. Most neutrons go through the monitor without interacting, due to the very low helium thickness.

Some of the neutrons capture on the helium 3 and produce an excited (compound) helium 4 nucleus which subsequently decays into a proton and a triton. Both the proton and triton then ionize the gas (mostly the Nitrogen) as they move through the monitor and the resulting electrons are carried away by the center plate anode. The two outer plates are held at 3 kV. The monitors operated as designed and the associated technology is a proven concept.

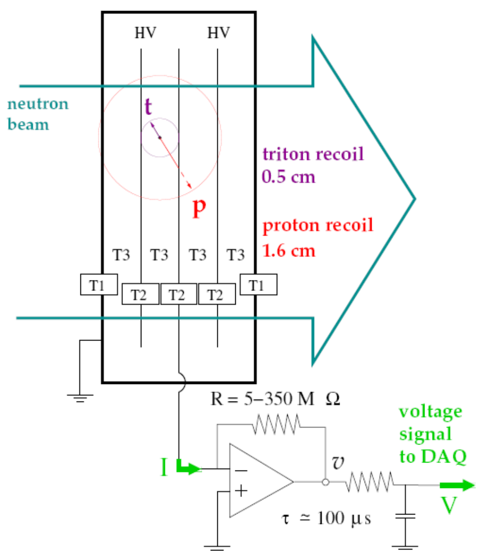

Figure 1

Figure 2: Schematic of the current NPDGamma beam monitors

To come as close as possible to counting statistics, an important requirement is that most of the protons (and tritons) range out and deposit most of their energy in the chamber, reducing the fluctuations in the signal. For the beam monitors, in which the distance between the plates is only 9.9 mm, this is achieved by having a gas mixture of 0.5 atm of Nitrogen, 0.47 atm of Helium 4 and 0.03 atm of Helium 3. The large Nitrogen content reduces the mean free path of the charged ions. This situation changes for the operation of the wire chamber, as described below.

4.2 The Target Wire Chamber

The principle behind the proposed wire chamber is the same as described above for the beam monitors, but there are some additional design considerations. Ideally, the chamber will be able to operate in two different modes. In mode one, the chambers are used to measure the PV asymmetry, while for mode two, the chambers could be reconfigured, such that they can measure PC left-right asymmetries and beam motion. The chamber then needs to have finite resolution in the directions transverse to the beam direction to detect left-right and up-down beam motion and asymmetries. In the primary mode, for the measurement the PV asymmetry, the chambers need to have good resolution in the beam direction, since the forward-backward asymmetry is to be measured here. For these reasons, the chamber needs to have wire planes for both the high voltage planes as well as the collector planes, instead of plates.

In contrast to the beam monitors above, which are supposed to absorb only a small amount of the neutron beam, the wire chamber needs to be completely black to cold neutrons. In other words, all of the neutrons in our energy range (see below) need to be captured in the chamber to obtain good counting statistics. To achieve this, the fraction of ^3He needs to be significantly larger. Initial design simulations were conducted with a mixture of 90% ^3He and 10% of another gas (Nitrogen or Hydrogen). The additional gas is only used to reduce the effect of breakdown (i.e. to increase the dielectric strength of the gas) at high voltages. Since the proton range in a chamber that is mostly filled with ^3He is about 4 cm, and the mean free path of the neutrons in our energy range is about 2.5 cm, the chamber needs to be about 20 cm long in the direction of the beam, to allow all protons to range out in the beam direction (note that the proton range increases with smaller amounts of dilution gas).

Figure 3 illustrates a possible design choice as well as several facts with regard to the proton-triton dynamics and relative signals. We envision the chamber to be a cube with a side length of about 20 cm. In the configuration shown, the chamber will be sensitive to variations in the deposited charge along the beam direction, since the signal wires in each plane are summed to produce one signal per plane. This summing of the signal will reduce the cost associated with DAQ electronics, by reducing the number of ADC modules.

Figure 3 also illustrates that the majority of the kinetic energy after fission of the ^4He nucleus is carried away by the proton (75% of it) and that most of the ionization occurs toward the end of the proton range. The chamber must be large enough to allow the proton to range out. This is another reason for the necessity of wires, since plates would not allow the proton to range out. For the purpose of measuring longitudinal asymmetries, the optimum sensitivity is reached when the neutron mean free path is small compared to the range of the proton.

4.3 Detector Efficiency Simulations and Error Dilution

The efficiency of the wire chamber depends in a complicated way on the proton angles, neutron energy, and wire plane spacing. The overall efficiency of the detectors σ_d will enter into the error on the physics asymmetry as $\sigma_d/\sqrt{N}$, where N is the total number of neutrons that capture in the target. The energy deposition by the proton and triton varies, based on where the neutrons capture. Neutrons which capture close to the entrance window of the chamber will have a large negative asymmetry (for a positive PV asymmetry), since the backward going protons are absorbed in the wall, before depositing most of their energy. Also, as shown below, the protons deposit most of their energy at the end of their range, so that the first few wire planes will not see as much energy deposited for forward going protons as compared to those that are emitted left-right. The

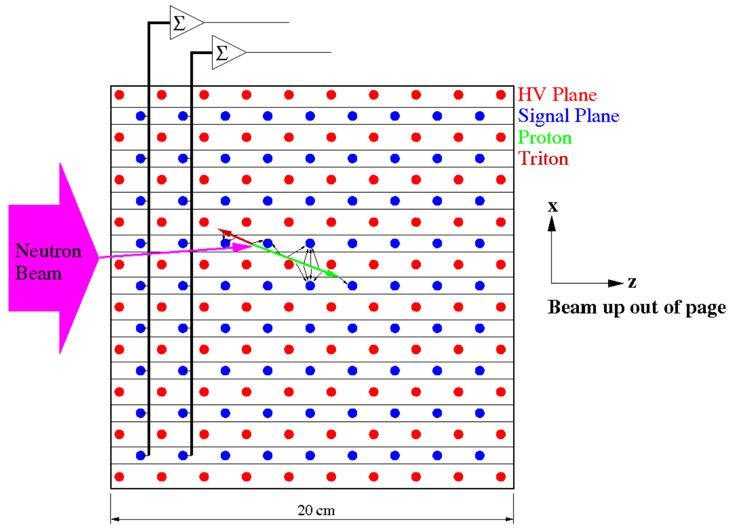

Figure 3: Initial design possibility for the target wire chambers.

parity violating longitudinal asymmetry in ^3He has the form, $A_p \cos\theta$, where $\cos\theta = \vec{k}_p \cdot \hat{z}/|\vec{k}_p|$ and therefore, protons of the ladder type have zero (or close to zero) PV asymmetry. However, the first few wire planes can, therefore be used to monitor the parity allowed (PC) left-right asymmetries as well as left-right beam motion. Since the bulk of the neutrons will capture in the front wire planes, these asymmetries can be measured to an accuracy, better than the PV asymmetry, in less time. This however, would require a reconfiguration of the wire summing. On the other hand, the first few wire planes can then also be used to normalize to the beam current. This is possible without much loss in accuracy for the PV asymmetry, since the first few wire planes are not very sensitive to the forward backward asymmetry.

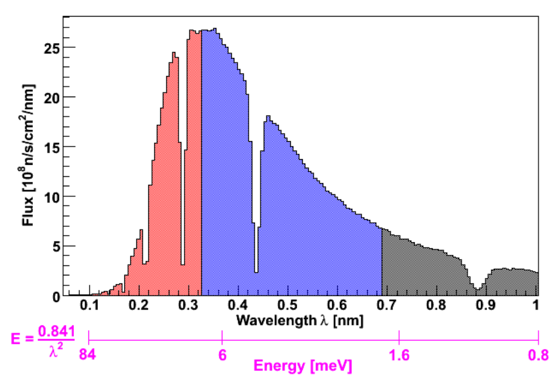

Figure 4: Simulated neutron spectrum for the SNS FNPB beam line [21]. The blue region indicates the optimized neutron energy range for this experiment.

The signals in different planes give some information on $\cos\theta$ because the protons with large $\cos\theta$ produce signals in planes with large z. Using this z information, the statistical accuracy, to which the asymmetry can be determined, can be obtained with a suitable Monte Carlo simulation. The Monte-Carlo optimization is needed to choose the optimal neutron wavelength interval and the optimum number and separation of wire planes, leading to a determination of the RMS width σ_d in $\delta A_p = \sigma_d/\sqrt{N}$. To determine the optimum gas mixture and field, additional simulations have to be performed, but the overall concept will not change. Slight changes in the wire spacing and number will also not affect the cost of the chamber significantly.

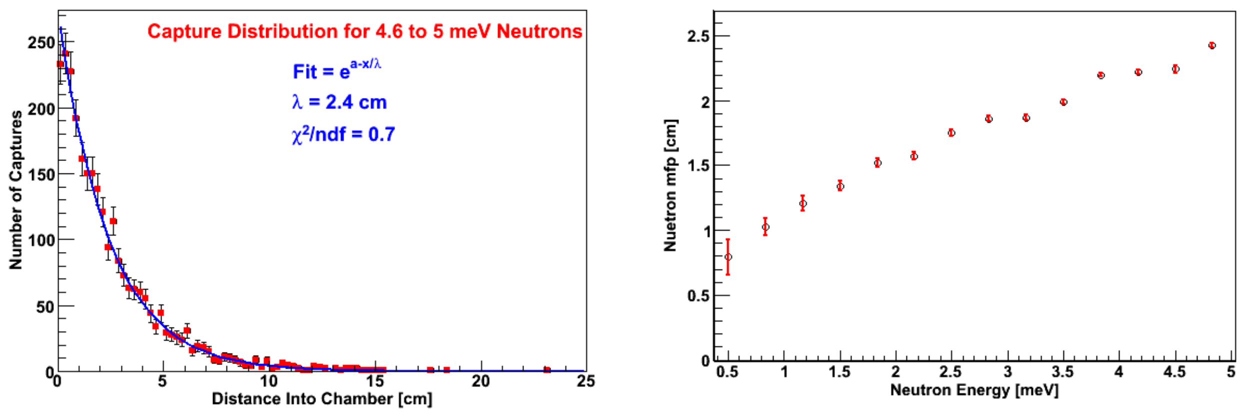

Figure 5: Neutron mean-free-path for 10% N and 90% ^3He, obtained from a bench-marked simulation (errors are from the simulation).

Two independent simulations were performed for the optimization. The first one, using Geant4, was properly bench-marked against data and was used to produce the graphs shown here. The second simulation [22] is a stand alone dedicated code, which includes a few additional analysis capabilities, such as neutron wavelength window optimization and the effects of correlations between wire planes. Both codes agree in the limit of no correlation. Final results for wavelength optimization and error calculations are based on a combination of both codes.

The goals of the simulations are to determine:

- the ionization response in each wire plane
- the sensitivity to the asymmetry in each wire plane
- the statistical error and correlations of the signals in each wire plane
- the requirements in digitizing the output signal
- the effective statistics of the helicity asymmetry and
- the feasibility of measuring a detector asymmetry to cancel beam fluctuations

The neutron spectrum in either simulation is based on figure 4, which shows the number of neutrons expected at the SNS [21], versus neutron wavelength, together with the best wavelength range, for which the neutron mean free path is less than the range of the proton (blue region). Note that, due to frame overlap with the 60 Hz SNS beam pulse rate, only a window of about 0.4 nm can be used for data taking. The exact location of the window is a matter of ongoing optimization. The simulation figures shown here used a maximum neutron energy of 5 meV, just after the Bragg edge. The neutron spectrum is based on a McStas simulation [23].

Figures 5 show the simulated neutron mean free path for a gas mixture of 10% Nitrogen and 90% ^{3}He. The properties of the proton in this gas mixture are shown in figure 6. Figure 7 shows a comparison of the simulated total stopping power for protons in pure ^3He to a curve for ^4He, based partially on data, taken from [24, 25]. A small fraction of additional gas is needed to prevent breakdown in the wire chamber. A 10% nitrogen content, however is on the high side. Since the range of the proton decreases significantly with nitrogen gas content, while the neutron range remains largely unaffected, the efficiency of the chamber will get worse with larger nitrogen content. Other possible gases include hydrogen and ^4He.

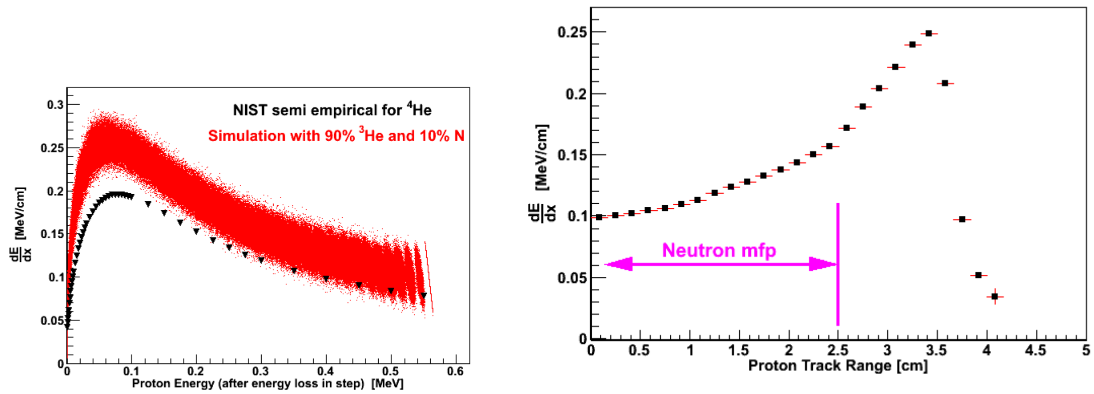

Figure 6: The proton starts on the left edge (right plot) with an energy of 571 keV and is seen (left plot) to loose more than half of its energy over the last 2 to 3 cm of its track, while the range of neutron mean free path (dependent on neutron energy) has a maximum of 2.5 cm for 5 meV neutrons (magenta).

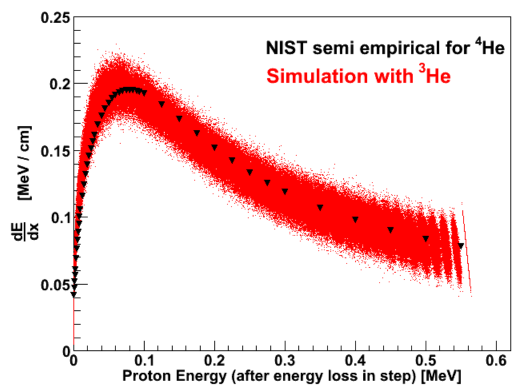

Figure 7: Proton energy loss for pure ^3He in the simulation, compared to the data available from NIST (used in benchmarking the simulation).

4.3.1 Detector Efficiency

Figure 8 shows the proton energy deposition for 2.5 meV neutrons as a function of proton angle (θ) with respect to the beam direction and as a function of distance into the target. The x-axis binning for the left-hand figure corresponds to a wire plane spacing of 5 mm. Similar graphs are obtained for other neutron energies, where neutrons with small energies tend to deposit their energy close to the front window. Figure 8 also shows the same two graphs for the triton energy deposition.

Note that the asymmetry in eqn. 2 involves two terms; one for the proton and one for the triton. If one considers that $A_T \simeq -A_p/3$ (because $k_T = k_p/3$, see eqn. 3), and using $f_p \equiv f_p(\theta, z, E_n)$, $f_T \equiv f_T(\theta, z, E_n)$ for the proton and neutron energy deposition distributions in z (the depth into the target), E_n (neutron energy) and θ, then the experimental asymmetry is

$$A_{exp}^{i,j} = A_{ph}^{i,j} \frac{\int (f_p - f_T/3) \cos\theta d\theta}{\int (f_p + f_T/3)\, d\theta} \ . \tag{5}$$

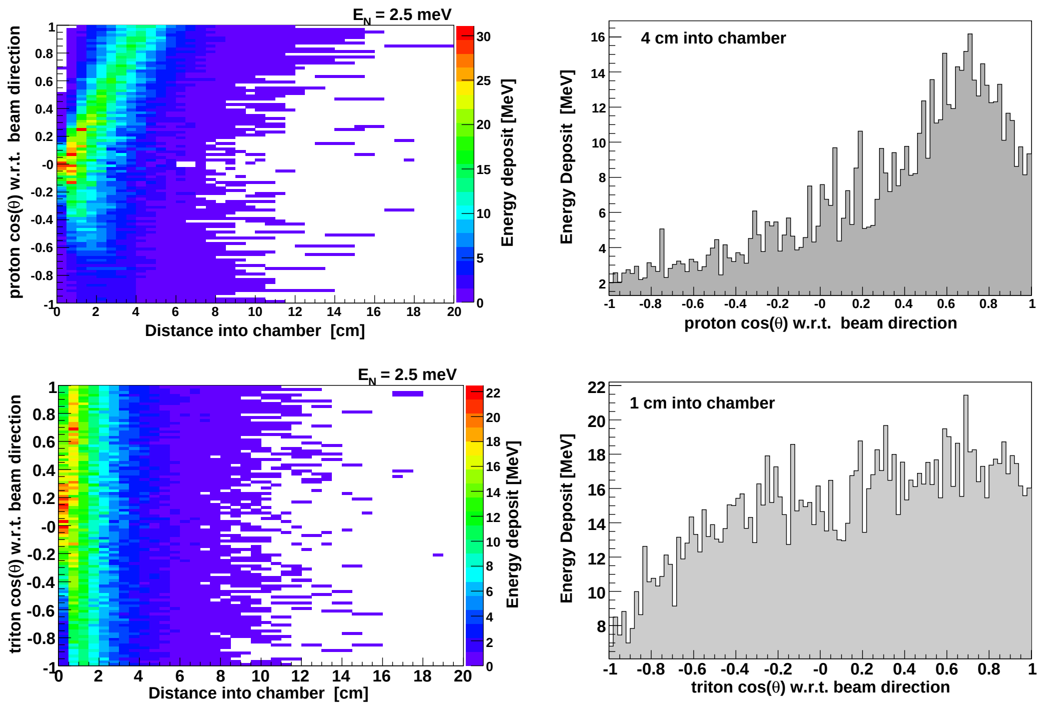

Figure 8: Simulation results for the angle and chamber depth dependence of the proton (upper plots) and triton (lower plots) energy deposition for 2.5 meV neutrons. In the left hand graphs, the neutron beam is moving to the right. The deposited energy has been summed up over several 100000 events for this neutron energy.

There is an additional factor of about 1/4, by which the triton portion is smaller, due to the fact that it only deposits 1/3 of the energy of the proton and the fact that this energy is deposited at the beginning of the track rather than the end, as is the case for protons. Figure 9 shows the number of ion pairs produced as function of triton and proton range. However that factor is implicit to the distribution obtained from simulation. Since proton and triton ion tracks are indistinguishable except for their range, we add the two functions, as shown in eqn. 5 and fig. 9. Then, Using the shorthand notation

$$\xi^{i,j}(z, E_n) \equiv \frac{\int (f_p(\theta, z, E_n) + f_T(\theta, z, E_n)/3)\, d\theta}{\int (f_p(\theta, z, E_n) - f_T(\theta, z, E_n)/3) \cos\theta d\theta}$$

we can write the error on the physics asymmetry as

$$\delta A^{i,j}_{exp} = \frac{\delta A^{i,j}_{ph}}{\xi^{i,j}(z, E_n)} = \frac{1}{\sqrt{N_{i,j}}}\sqrt{1+\sigma^2_{coll}}\ , \tag{6}$$

Here, the indexes (i, j) run over all z-bins (binned depth into the chamber) and all neutron energy bins respectively, σ_{coll} incorporates the RMS widths associated with collecting the signal from the wire chamber, and $N_{i,j}$ is the number of neutron captures in wire plane i for neutron energies contained within the jth energy bin. The error on the physics asymmetry for $N_{i,j}$ captures with neutron energy E_n in wire plane z is then

$$\delta A^{i,j}_{ph} = \frac{1}{\sqrt{N_{i,j}}}\xi^{i,j}(z, E_n)\ . \tag{7}$$

The quantity σ_{coll} is the quadrature sum of noise sources such as electronic noise, charge collection noise in the chamber, and beam noise. Based on previous experience at LANSCE, we expect those sources to be at least an order of magnitude smaller than the RMS width expected from counting statistics. The factor $\xi^{i,j}(z, E_n)$ produces the largest increase in error by far and we ignore σ_{coll} for the moment.

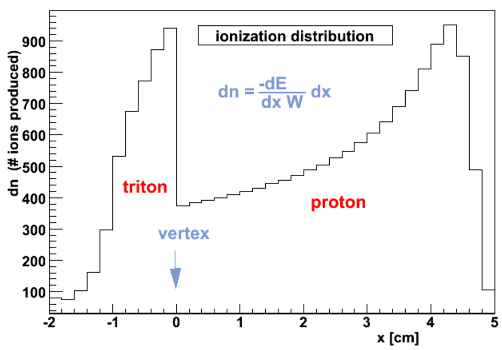

Figure 9: Simulated proton and triton ion pair production as a function of range.

Performing an error weighted average over the wire planes and neutron energy bins then provides the final physics asymmetry error for a given total number of events $N = \sum_i \sum_j N_{i,j}$ incident on the target

$$\delta A_{ph} = \frac{1}{\sqrt{\sum_i \sum_j \frac{N_{i,j}}{(\xi^{i,j}(z,E_n))^2}}}. \tag{8}$$

Normalized to the total number of events, this becomes

$$\sigma_D = \frac{\sqrt{N}}{\sqrt{\sum_i \sum_j \frac{N_{i,j}}{(\xi^{i,j}(z,E_n))^2}}}. \tag{9}$$

Which is now written as a RMS width detector efficiency.

This quantity, which we refer to as the error dilution due to detector inefficiencies was calculated using the simulation. The error for the asymmetry is then

$$\delta A_{ph} = \frac{1}{\sqrt{N}P_N}\sqrt{\sigma^2_D + \sigma^2_{coll}}\ . \tag{10}$$

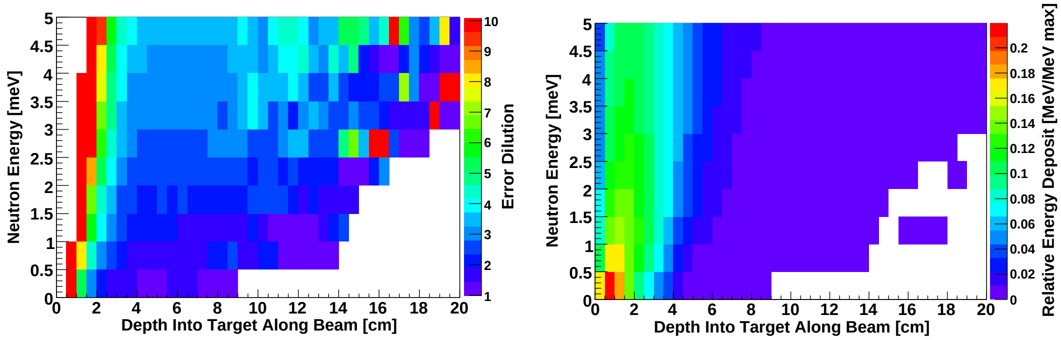

Figure 10: Left: Error dilution versus distance into target along beam and neutron energy. Right: Relative energy deposition. Note that there are few events for the higher energy and larger target depth bins, and that the high error dilution bins there are a reflection of poor statistics rather than actual detector efficiency. Generally, the efficiency is higher for events that occur at larger depth into the target.

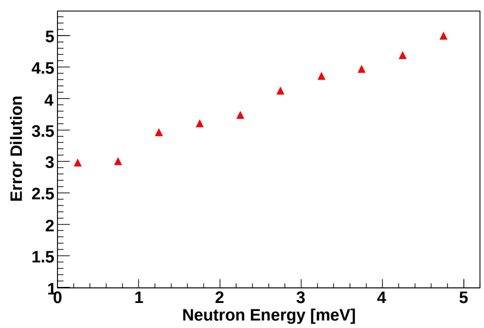

Figure 11: Combined error dilution as a function of neutron energy. The error dilution grows with neutron energy, since the mean free path of the neutron grows, whereas the proton range remains constant.

Figure 10 shows the dilution (σ_D) as a function of depth into the chamber and neutron energy compared to the relative energy deposition. Figure 11 shows the dilution for all events in the chamber as a function of neutron energy. The weighted mean combined dilution is $\sigma_D \simeq 4$. This result is modified somewhat by effects of wire plane correlation signal, as described in the next section. The error dilution grows approximately linearly with neutron energy which is a result of the fact that the mean free path of the neutrons grows as a function of their energy, whereas the proton range remains constant. From the point of view of error dilution, the best range for the proton asymmetry measurement is between 3 and 14 cm into the chamber. However, it is found that the large energy weight in first few wire planes makes a statistically significant contribution and can be used as a beam current normalization, since the sensitivity to the longitudinal asymmetry is small there.

4.3.2 Wavelength Window Optimization and Wire Plane Correlation

A ballistic neutron transport simulation has been performed to optimize the measurement of the asymmetry with respect to the neutron wavelength window and wire plane spacing. Additional analysis, including correlation between wire planes, is included. For each capture vertex $(z, \cos(\theta))$, we calculate the ionization distribution due to the proton and triton recoil energy using $\beta_{p,t}(x) = dn_{ion}/dx$, the ion density as a function of the distance the proton or triton has traveled. Since proton and triton ion tracks are indistinguishable except for their range, we add the two functions. (Note that this is explicitly stated here for the dedicated code referenced above. Geant4 has this as a built in process.) A detailed description of the code and calculations is given in [22].

To optimize the wavelength window for the SNS, the simulation calculates $\delta A^{-2} = N/(\sigma_d)^2$, corresponding to a single neutron pulse, (multiplying by 60 Hz $\times 10^7$ s produces the final weight δA). The results are summarized in table 2.

Neutron Wavelength Window Optimization			
Chopping Phase (at 17 m)	σ_d	δA^{-2} ($\times 10^6$)	Comments
244	???	1.259	
234	6.60	1.29	
244	6.55	1.31	
254	6.51	1.33	
284	6.33	1.35	
300	6.24	1.356	$\lambda \simeq 0.3 \rightarrow 0.69$ nm
320	6.10	1.35	
360	5.8	1.311	
500	5.0	1.019	

Table 2:

Then, using the optimal chopping phase of 300 degrees ($\lambda = 0.3 \rightarrow 0.69$ nm) (at 17 m), the number of wire planes and distance between them was varied, both with and without taking into account the correlation between wire planes. If correlations are not taken into account, then σ_d drops, indicating double-counting. The results are summarized in table 3.

Effect of Wire Plane Spacing on Correlations			
Wire Planes	Width [mm]	σ_d (no correlation)	σ_d (with correlation)
10	20	5.27	6.24
20	10	4.19	5.97
40	5	3.37	5.90

Table 3:

4.3.3 Conclusions from Simulations

From error considerations alone, the optimal wavelength window and wire plane spacing appears to be ($\lambda = 0.3 \rightarrow 0.69$ nm) and 5 mm respectively, leading to an error dilution of

$$\sigma_d \simeq 6 \ . \tag{11}$$

Figure 12 illustrates a possible configuration of the first two choppers at the SNS, to accommodate this window (the information on the chopper specification has been taken from [21]). It is assumed that the experiment will be located about 17 meters from the cold moderator.

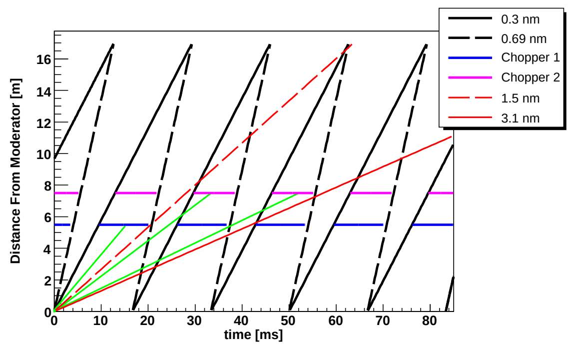

Figure 12: A diagram of the phasing of choppers 1 and 2 at 5.5 and 7.5 meters from the cold moderator, illustrating how to accommodate the chosen wavelength window. The width of the window is constrained by the 60 Hz repetition rate at the SNS. The wavelength range can be adjusted arbitrarily by re-phasing the choppers [26].

Additional simulations are needed to optimize the wire plane spacing with respect to charge collection and other properties, however, as seen in table 3, the variation in σ_d, with the spacing, is not very strong and no significant changes in the error dilution are anticipated. We can therefore say that making this measurement with a wire chamber of the basic design described herein, constitutes a viable experiment.

5 Spin Flipper / Rotator

Since the experiment is run in longitudinal polarization mode, a new RFSF will have to be designed with a transverse RF B-field. The current design is a double-racetrack wave guide with the active region in the center as illustrated in Fig. 13. The RF coils are placed in the two outer loops out of the way of the neutron beam. The B-field lines of the RF mode excited by this geometry run in circles around each loop, parallel to each other in the spin flip region. The purpose of the two separate tracks is to cancel gradients to first order in the middle, and also to allow for efficient driving of the waveguide. The interaction region would be a 15 cm cube, making the whole RFSF about 75 cm $\times$ 75 cm $\times$ 15 cm.

6 Statistics and Flight Path Time Request

The neutron capture cross section in ^3He is large and the cross-section $\sigma \simeq \sigma_o/v$. The longitudinal asymmetry, $\delta A_{ph}/A_{ph}$ is independent of neutron energy. We estimate the statistical uncertainty

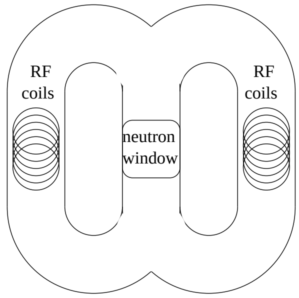

Figure 13: A cross section of the current design for a longitudinal RFSF. The double-racetrack design allows for efficient generation of B-fields, without interference with the neutron beam. The outside dimensions are 75 cm $\times$ 75 cm $\times$ 15 cm.

in the measurement as follows. Starting from figure 4, we take the neutron flux from FNPB to be 9×10^{10} neutrons per second at 1.4 MW [21]. About 6.5×10^{10} neutrons fall within the frame shown in blue, in figure 4 (assuming a 10 cm by 12 cm guide cross-section). About 30% of the neutrons make it through the super-mirror polarizer, with 96% polarization. In addition, we need two pulses to measure a single asymmetry, so the number of neutrons for statistics is reduced by an additional factor of 2. We also assume that there will be another 10% of attenuation losses. This information is summarized in table 4.

Neutron Event Rate In The Detector		
Source	amount/fraction	total/sec
Neutrons from beam		6.5×10^{10}
Polarizer transmission	$\times 0.3$	1.9×10^{10}
Attenuation	$\times 0.9$	1.7×10^{10}
Two pulses per asym.	$\times 0.5$	8.7×10^{9}

Table 4:

In a 1×10^7 sec run we will then observe the interaction of about 8.7×10^{16} neutrons. We use the detector error dilution determined from simulations $\sigma_d \simeq 6$, as shown above. So in that time, we can measure the asymmetry to

$$\frac{6}{0.96\sqrt{8.7 \times 10^{16}}} \simeq 2 \times 10^{-8} \ ,$$

which would be a 7% measurement of the estimated 3×10^{-7} asymmetry. Even if the asymmetry is entirely in the scattering states (which is unlikely), producing the 5×10^{-8} asymmetry estimate, we can still measure the asymmetry with a statistical uncertainty of about 40% in that time, which would be a competitive measurement in the hadronic weak interaction world.

In order to allow for setup, commissioning, and to account for possible beam interruptions and other technical problems, causing breaks in production running, we request a period of one year on the beam line.

7 Systematic Effects

The measurement will be done by reversing the neutron spin direction in fixed detector geometry and observing the change in the detector yield. Cartesian invariants that do not involve the spin, do not produce detector asymmetries. Since $\sigma_i\sigma_j = \delta_{ij} + i\epsilon_{ijk}\sigma_k$, we only need to consider cartesian invariants that are linear in $\vec{\sigma}_n$, the spin of the neutron. The remaining independent vectors in the problem are $\vec{k}_n$ and $\vec{k}_p$ ($\vec{k}_T = -\vec{k}_p$). The various relevant spin and momentum combinations are shown table 5.

Invariant	Parity	Size	Comments
$\vec{\sigma}_n \cdot \vec{k}_p$	Odd	1×10^{-7}	RMS value
$\vec{\sigma}_n \cdot (\vec{k}_n \times \vec{k}_p)$	Even	$2 \times 10^{-6} \times 10^{-2} \times 10^{-2}$	size times alignment factors
$\vec{\sigma}_n \cdot \vec{k}_p(\vec{k}_n \cdot \vec{k}_p)^m$	Odd	$k_n r = 3.7 \times 10^{-5}$	gets smaller by 10^{-5} for each additional power (m)
$\vec{\sigma}_n \cdot (\vec{k}_n \times \vec{k}_p)(\vec{k}_n \cdot \vec{k}_p)^m$	Even	$k_n r = 3.7 \times 10^{-5}$	gets smaller by 10^{-5} for each additional power (m)
$\vec{\sigma}_n \cdot \vec{B}$	Even		Stern-Gerlach steering: analysis in progress
$\vec{\sigma}_{^3He} \cdot \vec{k}_p$ or $\vec{\sigma}_{^3He} \cdot \vec{k}_n$	Even		Polarization of ^3He: small effect, can be countered with magnetic holding field reversal
$\vec{\sigma}_n \cdot (\vec{E} \times \vec{v_n})$	Even	1×10^{-4}	Mott-Schwinger Scattering for transverse polarization only

Table 5:

Both the radius of ^3He ($\simeq$ 1.7 fm) and the range of the strong interaction ($\simeq$ 1.0 fm) are small. For a 10 meV neutron, $k_n r_{^3He} = 3.7 \times 10^{-5}$. For a 550 keV proton, $k_p r_{^3He} = 0.29$. For each additional power of m (see table), the size of the higher-order terms decreases by about 10^{-5}. The higher-order terms ($m > 0$) can, therefore, be neglected for both the PV and PC asymmetries. We have estimated the size of the PV asymmetry to be $O(10^{-8}) \rightarrow O(10^{-7})$ above.

The dimensional estimate of the parity-even term is $\vec{\sigma}_n \cdot (\vec{k}_n \times \vec{k}_p) \simeq 10^{-5}$. A calculation [27] of the parity-even asymmetry (A_{PA}), based on phase shifts using fits to data in the framework of R-matrix theory gives $A_{PA}(p/2) = (-1.7 \pm 0.3) \times 10^{-5}\sqrt{E_n/1\text{eV}}$.At $E_n = 10$ meV, the asymmetry is $A_{PA} = (-1.7 \pm 0.3) \times 10^{-6}$, or about 6 times smaller than the dimensional estimate. The goal statistical error of the measurement is $\simeq 2 \times 10^{-8}$. Therefore in order to make the false asymmetry less than 1/3 of the goal statistical uncertainty, the symmetry of the apparatus must suppress the parity-even asymmetry by about 1000.

7.1 Estimate of the False, Parity Allowed Asymmetry

The parity-even asymmetry vanishes if either σ_n or k_p is parallel to k_n. If σ_n is parallel to k_n, then the parity-even asymmetry can be reduced by two small numbers. For small angles, the experimental false asymmetry can be written as $A_{PA}^{exp} \simeq A_{PA}\theta_{k_p,k_n}\theta_{\sigma_n,k_n}$. Where θ_{k_p,k_n} is the angle between the proton momentum and the neutron momentum, and θ_{σ_n,k_n} is the angle between the neutron spin and the neutron momentum. We will measure the direction of k_n with a scanning ion chamber at two distances along the beam and align the plates of the ion chamber to be normal to k_n with an accuracy of 10^{-2} rad. We will also align the magnetic guide field and σ_n to be parallel to k_n with the same accuracy. The systematic uncertainty in A_{PV}, due to this effect, is given by $\delta_{A_{PV}} < 1.7 \times 10^{-6} \times 10^{-2} \times 10^{-2} = 1.7 \times 10^{-10}$. This value is 28 times smaller than the goal statistical error.

7.2 Left-Right Asymmetry from Mott Schwinger Scattering

Moving through the electric field of a molecule or atom, the neutron sees an effective magnetic field $\vec{B} = \vec{E} \times \vec{v}$ and experiences an interaction of the form $H' = -\vec{\mu} \cdot \vec{B}$. The analyzing power for a spin-less target can be calculated from the S-matrix, which is related to the coherent $g(\theta)$ and incoherent $h(\theta)$ scattering amplitudes.

$$S = g(\theta) + ih(\theta)\vec{s} \cdot \vec{n}$$

Here, θ is the scattering angle of the neutron (distinct from above), $\vec{s}$ is the spin of the neutron and $\vec{n}$ is the normal to the scattering plane. For completely transverse polarization, the Mott-Schwinger analyzing power is very large [28] (see fig. 14).

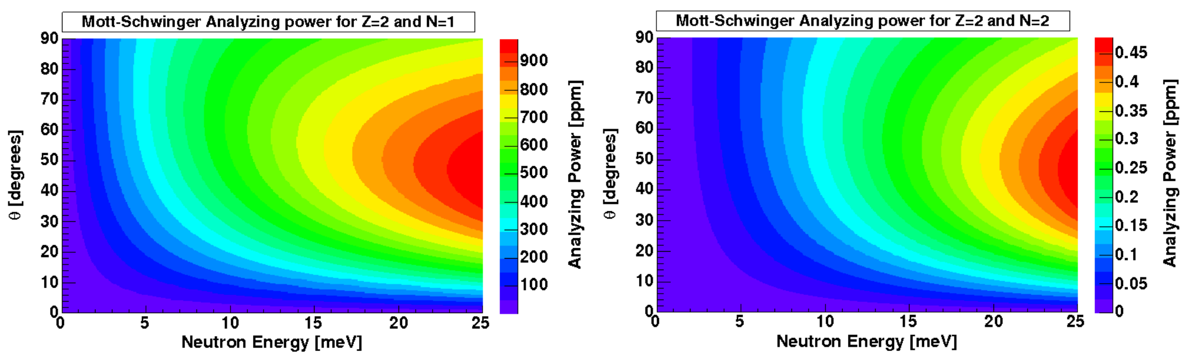

Figure 14: Analyzing power for ^3He (left) and ^4He (right) with electron screening. The magnitude of the analyzing power is shown. The sign of the asymmetry is negative.

However, for perfect longitudinal polarization, the S-matrix (and therefore the analyzing power) can be seen to vanish. The amount of transverse polarization is expected to be small and can be measured in auxiliary runs, using polarized ^3He analyzer cells. To reduce this effect below the goal statistical error, the alignment of the apparatus with the beam axis, must produce a factor of 100 suppression in addition to the suppression due to small transverse polarization components. A detailed analysis of this effect is currently underway.

8 Status, Funding, and Projected Budget

We are actively investigating the remaining systematic effects. We are also further optimizing and exploring additional target-detector chamber design options. A request for funding to build the wire chamber has been submitted to the Canadian funding agency NSERC, in October 2007. A super-mirror polarizer is being ordered for the FNP beam line. In the case of approval by the PRAC, we will begin to pursue the development of the holding field coil for the experiment and the spin flipper/rotator. Table 6 below summarizes our estimated budget.

Budget Estimates		
Major Equipment	cost	comments
Wire chamber	\$60k	requested
Spin flipper	\$30k	
Holding field	\$50k	
Data Acquisition	\$80k	we may be able to recycle some from NPDGamma

Table 6:

9 Future Plans (The $\mathbf{n} + {}^3\vec{\mathbf{He}} \rightarrow \mathbf{p} + \mathbf{T}$ Measurement)

We are considering a second generation experiment to measure A_p from the reaction $\mathrm{n} + {}^3\vec{\mathrm{He}} \rightarrow \mathrm{p} + \mathrm{T}$. This experiment would be sensitive to a different combination of coupling constants than the one described above. We must rely on the full 4-body calculation [17] of A_p to determine the sensitivity to each coupling constant. Qualitatively, the ^{3}He ground state is dominated by a spatially symmetric S wave in which the proton spins cancel and the spin of the ^{3}He nucleus is carried by the unpaired neutron[29, 30]. Therefore, $^3\vec{\mathrm{He}}$ is an effective polarized neutron target, and we expect $\mathrm{n} + {}^3\vec{\mathrm{He}} \rightarrow \mathrm{p} + \mathrm{T}$ to have similar features as n-$\vec{\mathrm{n}}$ scattering. In contrast, the reaction $\vec{\mathrm{n}} + {}^3\mathrm{He} \rightarrow \mathrm{p} + \mathrm{T}$ would be more sensitive to protons in the ^{3}He nucleus. It remains to be seen how much this qualitative behavior is modified by nuclear effects.

Similar to the setup described above, this experiment would use a ^{3}He cell as both the target and ion chamber detector. The difference is that the ^{3}He target would be polarized by optical pumping instead polarizing neutrons with the super-mirror bender. The 70% absorption of neutrons in the super-mirror bender would be avoided at the expense of lower polarization in the ^{3}He target. The effective statistics would be the same if ^{3}He polarization of $P_3 = 0.52$ can be achieved. A combination $^3\vec{\mathrm{He}}$ target/ion chamber has previously been used to study polarized muon capture on ^{3}He at LANSCE and TRIUMF [31]. New technology exists for efficient pumping of ^{3}He cell, and development of the target would focus on achieving $P_3 > 50\%$ in a target large enough to span the entire 10 cm $\times$ 12 cm cross section of the FnPB guide.

References

[1] M.J. Ramsey-Musolf and S.A. Page, Hadronic Parity Violation: A New View Through the Looking Glass Ann. Rev. Nucl. Part. Sci 56:2-52 (2006, in press)

[2] J. Erler and M.J. Ramsey-Musolf, Low Energy Tests of the Weak Interaction, Prog.Part.Nucl.Phys. 54 (2005) 351-442

[3] W.M. Snow, Neutron Measurements and the Weak Nucleon-Nucleon Interaction, J. Res. Natl. Inst. Stand. Technol. 110, 189-194 (2005)

[4] Y. Abov *et al.*, Phys. Lett. **25** 1964

[5] P. Herczeg, Second-Class Currents, Neutral Currents, and the Strangeness-Conserving Nonleptonic Weak Interactions, Phys. Rev. D 4, 1239 (1971)

[6] P. Herczeg and L. Wolfenstein, Symmetry Considerations for Parity-Violating Effects in the $n + p \rightarrow d + \gamma$ Reaction, Phys. Rev. D 8, 4051 (1973)

[7] P. Herczeg and P. Singer, Exchange effects from weak radiative mesonic transitions in parity-violating nuclear processes, Phys. Rev. D 11, 611 (1975)

[8] B. Desplanques, J. F. Donoghue and B. R. Holstein, Unified Treatment of the Parity Violating Nuclear Force, Annals of Physics, 124:449-495,1980.

[9] S.L. Zhu, S.J. Puglia, B.R. Holstein, M.J. Ramsey-Musolf, Phys. Rev. D 62 (2000) 033008.

[10] U. van Kolck, private communication

[11] E. G. Adelberger and W. C. Haxton, Parity Violation in the Nucleon-Nucleon Interaction, Ann. Rev. Nucl. Part. Sci., 35:501-558, 1985.

[12] S.L. Zhu *et al.*, Nuclear Physics A 748 (2005) 435-498

[13] W. Haxton and C. E. Weiman, Ann. Rev. Nucl. Part. Sci. 51, 261-293 (2001).

[14] W. Haeberli and B. R. Holstein, nucl-th/9510062, W. C. Haxton and E. Henley, eds., Symmetries in Nuclear Physics (1995).

[15] G. Mitchell, J.D. Bowman, S.I. Penttila, and E. Sharapov, Physics Reports 354, 2001

[16] V.E. Bunakov, V.P. Gudkov, Parity Violation and Related Effects In Neutron-Induced Reactions, Nucl. Phys. **A 401** (1983) 93-116

[17] M. Viviani, private communication, 2007

[18] Tilley et al. Nuclear Physics A 541 (1992)

[19] J. Carlson *et al.*, Parity-violating interaction effects: The longitudinal asymmetry in pp elastic scattering, Phys. Rev. C 65, 035502 (2002)

[20] R.C. Gillis, ^3He Ionization Chambers as Neutron Beam Monitors for the NPDGamma Experiment, M.Sc. Thesis (2006)

[21] P.R. Huffman *et al.*, NIST J. Res. 110, 161-168 (2005).

[22] C. Crawford, n3He Simulation Code,
http://sns.phys.utk.edu/svn/npdg/trunk/simulations/sns/choppers/tex/n3he_sim.pdf

[23] C. B. Crawford, unpublished technical note,
"McStas Bender Optimization for the NPDG cold line", 2007-10-04.
http://sns.phys.utk.edu/svn/npdg/ trunk/simulations/sns/choppers/tex/pol_bender.pdf

[24] M.J. Berger, J.S. Coursey, M.A. Zucker and J. Chang, NIST PSTAR program, http://physics.nist.gov/PhysRefData/Star/Text/contents.html

[25] ICRU (1993) International Commission on Radiation Units and Measurements. ICRU Report 49, Stopping Powers and Ranges for Protons and Alpha Particles.

[26] C. B. Crawford, R. Mahurin, unpublished technical note, “Opening angles for the SNS FnPB choppers”, 2006-11-30.

[27] G. Hale, LANL. Private communication

[28] M.Gericke, J.D. Bowman, and M. Johnson, Mott-Schwinger Scattering of Polarized Cold and Thermal Neutrons, Submitted to Phys. Rev. C. (2007)

[29] B. Blankleider and R.M. Woloshyn, Phys. Rev. C **29**, 538 (1984).

[30] J.L. Friar *et al.*, Phys. Rev. C **42**, 2310 (1990).

[31] P. Bogorad *et al.*, Nucl. Instrum. Meth. A **398**, 211 (1997).